High-Visibility On-Chip Quantum Interference of Single Surface Plasmons

Yong-Jing Cai, Ming Li, Xi-Feng Ren,* Chang-Ling Zou, Xiao Xiong, Hua-Lin Lei, Bi-Heng Liu,† Guo-Ping Guo,‡ and Guang-Can Guo

Key Lab of Quantum Information, University of Science and Technology of China, CAS, Hefei, Anhui 230026, People's Republic of China

Synergetic Innovation Center of Quantum Information & Quantum Physics, University of Science and Technology of China, Hefei, Anhui 230026, People's Republic of China

(Received 6 February 2014; revised manuscript received 19 June 2014; published 14 July 2014)

In this work, the on-chip quantum interference of two single surface plasmons is achieved using dielectric-loaded surface-plasmon-polariton waveguides. The high visibility (greater than 90%) proves the bosonic nature of single plasmons and emphasizes the feasibility of achieving basic quantum logic gates for linear optical quantum computation. The effect of intrinsic losses in plasmonic waveguides with regard to quantum-information processing is also discussed. Although the influence of this effect is negligible in the current experiment, our studies reveal that such losses can dramatically reduce quantum-interference visibility in certain cases; thus, quantum coherence must be carefully considered when designing quantum photonic integrated circuit devices.

DOI: 10.1103/PhysRevApplied.2.014004

I. INTRODUCTION

Photonic integrated circuits (PICs) attract considerable attention because of their small footprints, scalability, reduced power consumption, and enhanced processing stability. In addition to their wide application in classical information processing, integrated photonic quantum logic gates and Shor's quantum factoring algorithm have been demonstrated on these chips [1,2]. More recently, much effort has been dedicated to surface plasmon polaritons (SPPs), which are electron-density waves excited at the interface between a metal and dielectric material [3] to further condense PICs beyond the diffraction limit. Not only can SPPs confine light at the nanoscale [4], they are also useful for integrated polarization-controlling devices [5,6]. Studies using periodic metallic hole arrays provide the first experimental evidence that quantum entanglement can be preserved in the photon-SPP-photon conversion process [7–9]. Furthermore, the nonclassical statistics of SPPs have been demonstrated using basic quantum Hong-Ou-Mandel (HOM) interference [10] in both long-range plasmonic waveguides (weakly confining waveguide) [11] and subwavelength metal plasmonic waveguides [12]. These studies indicate that assembling quantum PICs (QPICs) using plasmonic components is possible.

However, two obstacles remain that hinder the development of SPP-based QPICs. The first is that the experimental raw visibility of the quantum interference realized in plasmonic waveguides is below 50% [12], which is the boundary between classical and quantum interference [13]. This low visibility is not compelling evidence that single plasmons are usable for quantum-information processing. Interference visibility is so important that higher quantum-interference visibility implies higher operation fidelity and a higher probability of success. For example, the HOM interference with 95% visibility that can be achieved in QPICs based on dielectric waveguides is used to realize quantum-controlled NOT gates [1]. Quantum interference with high visibility can also be used to prove the bosonic nature of single surface plasmons, which was first discussed in works of surface plasmon amplification by stimulated emission of radiation (Spaser) [14,15]. Second, loss is unavoidable in QPICs that are based on plasmonic waveguides [4] because of the absorption of metals. Although the properties of lossy quantum channels have been recently observed and studied in the context of free-space quantum optics [16,17], the influence of such losses on quantum processing using QPICs remains unknown [18,19].

The current study experimentally achieves the on-chip quantum interference of single plasmons using dielectric-loaded plasmonic waveguides at telecom wavelengths. The visibility is as high as $95.7\% \pm 8.9\%$, which unambiguously demonstrates the bosonic nature of single plasmons and paves the way for the performance of basic quantum operations in plasmon-based QPICs. Furthermore, a SPP waveguide might provide a perfect testing ground for studying lossy photonic devices because of the relatively high loss of such devices compared with dielectric devices. Our analysis indicates that subwavelength plasmonic components can be used as quantum devices for QPICs only when the loss effect is carefully addressed because loss can significantly reduce quantum-interference visibility. Because loss is inevitable in waveguides, it is necessary to consider its influence on quantum coherence when designing QPIC structures.

*renxf@ustc.edu.cn
†bhliu@ustc.edu.cn
‡gpguo@ustc.edu.cn

II. THE PRINCIPLE OF QUANTUM INTERFERENCE AND EXPERIMENTAL DESIGN

HOM interference [10], a basic type of quantum interference that reflects the bosonic properties of a single particle, is generally used to test the quantum properties of single plasmons. In addition to its fundamental importance within quantum physics, the HOM effect underlies the basic entanglement mechanism in linear optical quantum computing [20].

HOM interference can be described as follows: When two indistinguishable photons enter a 50:50 beam splitter (BS) from different sides at the same time, the two photons will come out together and never be in different output ports. This phenomenon is a signal of photon bunching and can only be explained using quantum mechanics [21]. Experiments typically control the arrival times of two photons by adjusting the path-length difference between them and measure the photon coincidence (the case that two photons arrive at two detectors simultaneously) of output port 1 (P1) and output port 2 (P2) of the BS. When two indistinguishable photons completely overlap at the BS, they give rise to the maximum interference effect and no coincidence exists. Visibility is defined as $V_1 = (C_{\max} - C_{\min})/C_{\max}$, where $C_{\max}$ is the maximum coincidence, and $C_{\min}$ is the minimum coincidence. For perfect quantum interference, $C_{\min} = 0$ and $V_1 = 1$, whereas for a classical coherent laser, $V_1 = 50\%$. Consequently, to prove that destructive interference is due to two-photon quantum interference, the visibility must be greater than 50%. Here, we use a modified HOM interferometer [see Fig. 1(a)]. We collect the photons from P2 of the first BS, send them to the second 50:50 BS, and then measure the coincidence. In this case, the visibility is modified as follows: $V_2 = (C_{\max} - C_{\min})/C_{\min}$. For perfect quantum interference, $C_{\max} = 2C_{\min}$ and $V_2 = 1$. Our modified interferometer is capable of reflecting the indistinguishability of the input particles and can tell us whether these plasmons are bosons.

Figure 1 gives the schematic of our experimental setup, in which the on-chip BS is the most important component. Here, we choose a dielectric-loaded SPP waveguide (DLSPPW) [22] to test the bosonic properties of the single plasmons. A DLSPPW is a typical subwavelength plasmonic waveguide that is formed by placing a dielectric ridge on top of a thin metal layer. DLSPPWs can confine the lateral size of propagating modes to the subwavelength scale and simultaneously transmit photons and electrons in the same component. Thus, highly efficient control of the waveguide-mode characteristics (such as high-speed power-monitoring [23] and switching [24] elements) is possible. We use nanofabrication techniques to prepare our plasmonic waveguide. Specifically, our waveguide is constructed of polymethyl methacrylate and placed on top of a 45-nm-thick gold layer deposited on a SiO_2 substrate. Figure 1(b) shows a SEM image of part of the fabricated sample.

Based on our calculations, the lateral size of the single-mode DLSPPW for photons at 1550 nm is

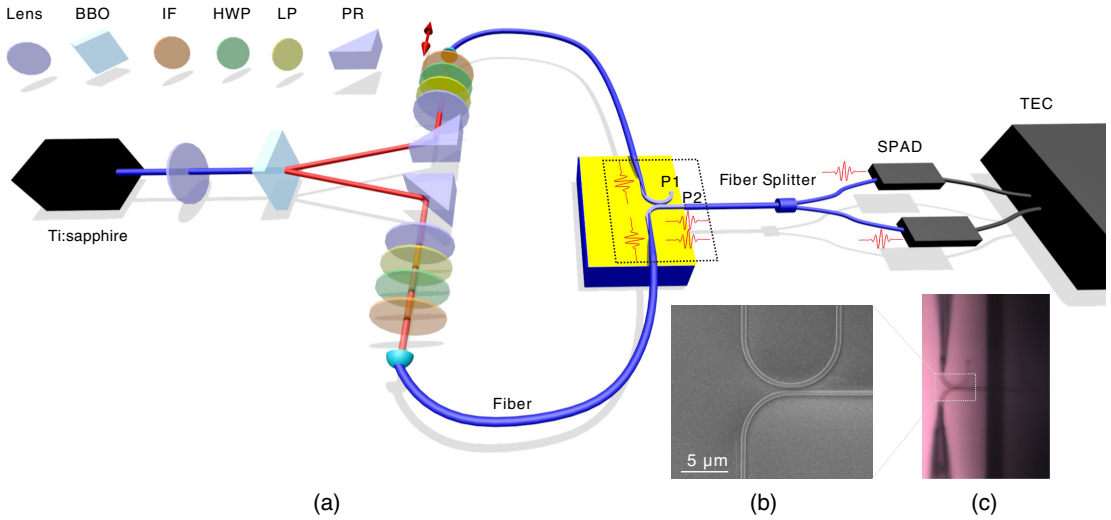

FIG. 1. (a) Schematic of the experimental setup. Photon pairs are generated via a degenerate type-II noncollinear spontaneous parametric down-conversion (SPDC) process. A 1.5-W pump laser (775 nm) is focused on a 1-mm-long BBO crystal. The produced twin photons (1550 nm) are separated in free space by a 6° angle based on the phase-matching condition and directed to different optical single-mode fibers. A motorized delay line in one of the arms allows the optical-path-length difference between the two photons to be controlled with 100-nm resolution. Using the fiber taper connected to the single-mode fiber, the single photons are converted into single plasmons in the plasmonic waveguide, which then interfere with each other. We collect the photons from P2 of the on-chip directional coupler (DC) and send them to a second 50:50 fiber BS. Coincidence measurements reveal the quantum properties of single plasmons. (b) A scanning electron microscope (SEM) image of part of a typical plasmonic DC structure. (c) A CCD image showing the coupling of the fiber taper and the SPP waveguide. A single-mode fiber is used to collect the photons from P2 using the end-fire coupling method.

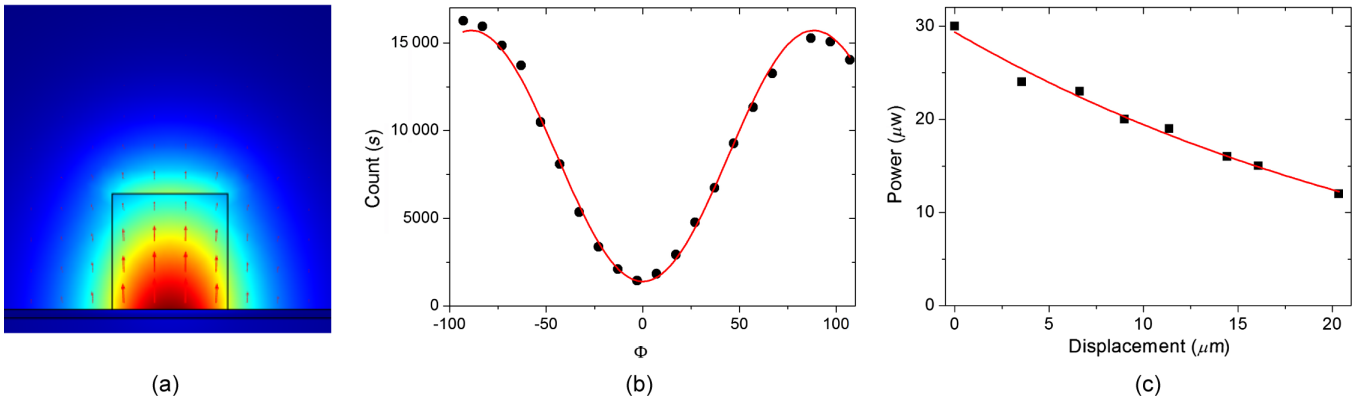

FIG. 2. (a) Field distribution in a single-mode plasmonic waveguide with lateral size of 600 nm × 600 nm. (b) The relationship between the output intensity of DLSPPW and the polarization of input photons. Φ is the angle between the polarization of input photons and the metal surface. When the polarization of incident photons is vertical to the metal surface, we get the maximum SPPs's excitation efficiency. (c) The relationship between the output intensity of DLSPPW and the propagation distance.

600 nm × 600 nm [25] [see Fig. 2(a)]. As we know, only photons polarized vertically to the interface between the metal and dielectric waveguide can excite SPPs in the DLSPPW. This polarization dependence is measured in our experiment. By rotating the half wave plate in the optical circuit, the polarization of input photons is changed. Then, we collect the photons from the output port of the DLSPPW with a single-photon detector. The results are shown in Fig. 2(b). The ratio between maximum and minimum counts is about 26 to 1, which proves that our DLSPPW has a good polarization-selective property. We also measure the propagation length of the single-mode DLSPPW. It is fitted to be 28 μm, which is smaller than the calculated value of 42 μm. Additional losses might arise from the nonsmoothness of waveguide surface produced during the nanofabrication process.

The BS is realized using a DC, which is composed of two waveguides, as shown in Fig. 3(a). In the coupling region, the evanescent fields of the two waveguide modes couple with each other and exchange energy. As a result, two new coupling eigenmodes—the symmetric [Fig. 3(b)] and antisymmetric [Fig. 3(c)] superpositions of the two waveguide modes—are generated. Because of their different effective refractive indices, the beating of the two modes leads to a BS-like function. By controlling the coupling strength, the amount of output at the two waveguide ports (the splitting ratio) can be tuned. In our experiment, many samples are fabricated, and the splitting ratios are measured using a laser working at 1550 nm. We excite the SPPs in the two input waveguides of the DC structures with the same incident power and measure the corresponding output power W_1 and W_2 from the output port P2 (see Fig. 1), respectively. The splitting ratio is defined as $S = W_1/W_2$. Since the gap of the DC sample has deviation due to the imperfection of the fabrication process, the splitting ratio of our samples is not constant, as shown in Fig. 3(d).

The coupling efficiencies among our SPP circuit, the external source, and the detectors are particularly crucial because the quantum signals are weak. However, it is difficult to directly connect our plasmonic waveguide to a single-mode optical fiber because its lateral-mode field area is much smaller than that of the fiber (diameter 6.8 μm). Therefore, we propose an adiabatic method [5,26] to excite the plasmons using a fiber taper [27,28]. As Fig. 1(c) shows, the photons in the fiber are adiabatically squeezed into the microfiber via the taper region and coupled to the plasmon waveguide when the microfiber approaches the waveguide. The tapered fiber is fabricated from a single-mode fiber (1550-nm wavelength) by heating it in the middle and stretching it from both ends. The cone angle of the taper is kept small so that the photons will propagate

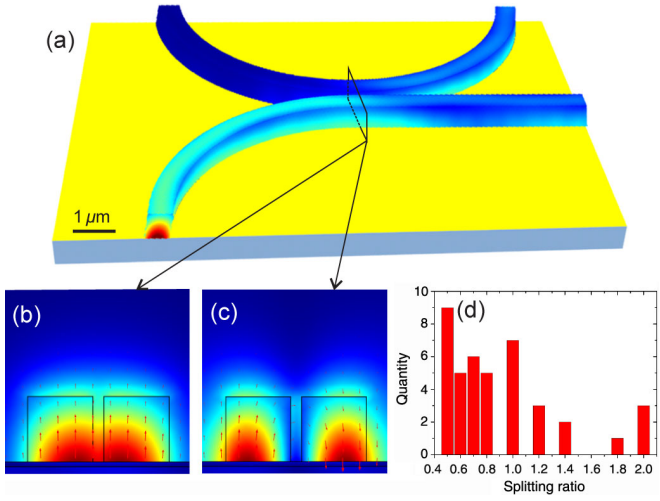

FIG. 3. (a) Three-dimensional simulation of the field distribution on our plasmonic DC structure. (b) Field distribution of the symmetric eigenmode in the coupling section. (c) Field distribution of the antisymmetric eigenmode in the coupling section. (d) The statistics of the splitting ratio of our samples.

adiabatically through the tapered region. The minimum diameter of our fiber taper fiber is approximately several hundred nanometers. By adjusting the contact area between the fiber taper fiber and the waveguide using a three-dimensional stage, we are able to efficiently excite plasmons. Because of the adiabatic conversion and evanescent field coupling, the ideal conversion efficiency might be higher than 99%. In our experiment, the overall efficiency $P = P_{\text{in}} \times P_{\text{loss}} \times P_{\text{out}}$, where P is the ratio of the output photons from the end-fire-coupled single-mode fiber to the input photons, P_{in} is the ratio of excited plasmons to input photons, P_{loss} includes the propagation loss, and P_{out} is the collection efficiency of the end-fire-coupled fiber. Under the limitations imposed by the experimental conditions, the efficiency of our fiber-taper-coupling system P_{in} is estimated to be approximately 30% [$P_{\text{in}} = P/(P_{\text{loss}} \times P_{\text{out}}) \sim 0.035/(0.201 \times 0.556) = 0.313$].

Another benefit of fiber-taper coupling is that plasmons can be generated in any region of the waveguide, not merely at the two ends (as in the objective-lens focusing method). This is useful when measuring propagation loss of the waveguide, as shown in Fig. 2(c). It should be noted that, for our DC, the alignment direction of the fiber taper is vertical to the collection fiber, thereby avoiding the collection of directly scattered photons from the end of the fiber taper. The ratio of signal to noise was above 100.

III. QUANTUM-INTERFERENCE RESULTS

The 1550-nm quantum photon pairs are generated via the spontaneous parametric down-conversion (SPDC) [29] process [see Fig. 1(a)]. The down-converted twin photons consist of one photon in the horizontal polarization and one in the vertical polarization. The photons are separated into two paths, each of which contains a prime reflector (PR), a half wave plate (HWP, 1550 nm), a long-pass filter (LP, 830 nm), and a narrow-band filter (IF, 1550 nm, 8.8 nm FWHM). After these components, the two photons, which now have the same polarization, are guided into two separate single-mode fibers. One of the fiber couplers is installed on a motorized stage to adjust the optical path.

As shown in Fig. 4(a), the indistinguishability of the produced photon pairs is first characterized using a standard HOM interferometer with a fiber BS. The dip represents the quantum interference of two photons, and the coherence of the photons determines its width. The quantum-interference results are fit using $N_{\text{HOM}} = C[1 - Ve^{-(\Delta\omega\Delta\tau)^2}]$ [10], where N_{HOM} is the measured coincidence count, C is a fitting constant, V is the quantum-interference visibility, $\Delta\omega$ is the bandwidth of the photons, and $\Delta\tau$ is the optical time delay. For perfect quantum interference of indistinguishable photon pairs, the visibility should be unity. Here, we obtain a visibility of $V = 95.5\% \pm 1.0\%$ and an optical coherence length of $c/\Delta\omega = 162.6\ \mu\text{m} \pm 5.0\ \mu\text{m}$, where c is the speed of light. The deviation of the visibility from 100% is attributed to the polarization distortion of the photons during propagation in the fiber, photon source variability, or both. We also test the modified quantum interferometer, in which photons from one output port are divided using a second fiber BS and detected with two single-photon detectors. Fitting the experimental results [Fig. 4(b)] using the function $N_M = C[1 + Ve^{-(\Delta\omega\Delta\tau)^2}]$, we obtain a visibility of $96.5\% \pm 3.1\%$ and a coherence length of $173.9\ \mu\text{m} \pm 5.7\ \mu\text{m}$. These values are consistent with standard HOM interference.

Finally, we observe the quantum interference of single plasmons using the modified quantum interferometer, in which two single photons from the fiber-excited plasmon pairs in separate waveguides and quantum interference occurs in the coupling section. We collect the photons scattered from P2 using an end-fire-coupled single-mode fiber. Using the second fiber BS, we divide the collected photons into two ports and measure the coincidence. Three samples are measured, and the visibilities are

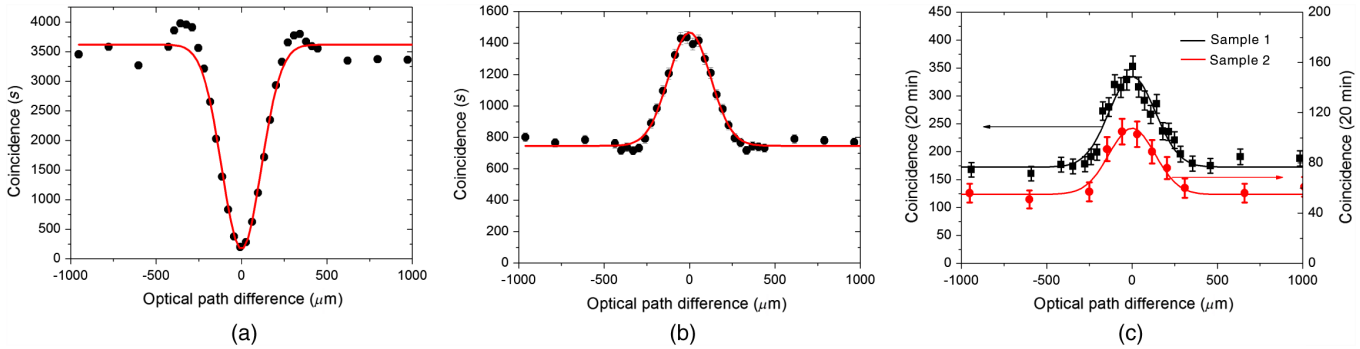

FIG. 4. (a) HOM interference of the down-converted photon pairs measured using a fiber 50:50 BS; the visibility is $95.5\% \pm 1.0\%$, and the optical coherence length is $162.6\ \mu\text{m} \pm 5.0\ \mu\text{m}$. (b) Quantum interference of the down-converted photon pairs measured using two fiber 50:50 BSs; the visibility is $96.5\% \pm 3.1\%$, and the optical coherence length is $173.9\ \mu\text{m} \pm 5.7\ \mu\text{m}$. (c) Quantum interference of single plasmons on DLSPPWs: For sample 1, the visibility is $95.7\% \pm 8.9\%$, and the optical coherence length is $191.6\ \mu\text{m} \pm 17.6\ \mu\text{m}$; for sample 2, the visibility is $93.6\% \pm 6.7\%$, and the optical coherence length is $193.0\ \mu\text{m} \pm 13.0\ \mu\text{m}$. All results are at the level of single photons.

95.7% ± 8.9%, 93.6% ± 6.7% [see Fig. 4(c)], and 93.1% ± 5.7%. These values are well above the classical limitation of 50%. The coherence lengths of the plasmons are also calculated using the experimental data yielding 191.6 μm ± 17.6 μm, 193.0 μm ± 13.0 μm, and 146.4 μm ± 9.4 μm, which are similar values to those of the photons. Our results demonstrate that although the electron is a fermion, a single plasmon (i.e., the quasiparticle of a collective electron-density wave) acts as a boson. The high visibility also suggests that plasmonic structures can be used in QPICs.

IV. DISCUSSION OF LOSS

In this section, we address the second question: What is the influence of loss on quantum-interference visibility? The following discussion provides a detailed account of the two-photon quantum interference of lossy channels based on our plasmonic DC structure.

The operation of a four-port DC can be described as follows:

$$\begin{pmatrix} b_1^\dagger \\ b_2^\dagger \end{pmatrix} = \begin{pmatrix} r & t \\ t & r \end{pmatrix} \begin{pmatrix} a_1^\dagger \\ a_2^\dagger \end{pmatrix}, \tag{1}$$

where $a_1^\dagger$ and $a_2^\dagger$ as well as $b_1^\dagger$ and $b_2^\dagger$ are the creation operators of the input and output boson particles, and r and t are the amplitudes of the reflection and transmission coefficients. The output state of the input twin-particle state $|1,1\rangle$ is

$$|\Phi\rangle_{\text{out}} = \sqrt{2}rt|2,0\rangle + \sqrt{2}rt|0,2\rangle + (r^2+t^2)|1,1\rangle \tag{2}$$

multiplied by a normalization factor. Here, we discard the terms that represent the loss of one or two particles because only the coincidence counts are recorded in the experiment. The probability of finding two boson particles in the same mode (proportional to the HOM interference visibility) is

$$P = \frac{4|rt|^2}{4|rt|^2 + |r^2+t^2|^2}. \tag{3}$$

For a lossless system, designing a DC with $|r|^2 = |t|^2$ should optimize quantum interference. However, for a lossy system, the structures and microscopic transport process of the DC will determine the second-order quantum coherence. In our DLSPPW DC, the precise microscopic losses can be included using the coefficients [30]

$$r = \frac{e^{in_2k_0L}}{2}\left(e^{i\mathrm{Re}(\Delta n)k_0L}e^{-\mathrm{Im}(\Delta n)k_0L} + 1\right), \tag{4}$$

$$t = \frac{e^{in_2k_0L}}{2}\left(e^{i\mathrm{Re}(\Delta n)k_0L}e^{-\mathrm{Im}(\Delta n)k_0L} - 1\right). \tag{5}$$

Here, $\Delta n = n_1 - n_2$, where $n_{1(2)}$ is the effective refractive index of the symmetric mode [the antisymmetric mode; see Figs. 2(c) and 2(d)], k_0 is the wave vector in free space, and L is the coupling length. The imaginary portion of $n_{1(2)}$ corresponds to the propagation loss of the plasmons and leads to a nonunitary operation matrix for the DC.

By substituting Eqs. (4) and (5) into Eq. (3), we obtain P, which is related to the loss difference between the two intermediate eigenmodes [$\propto \mathrm{Im}(\Delta n)$] and the coupling length L. When L is sufficiently large, P decreases to 0.5, which corresponds to a classical random process.

Figure 5(a) illustrates the relationships among P and L for a lossless DC (black dots), our DLSPPW DC (blue dots), and a metal-strip DC (red dots), in which we select the L that corresponds to a 50:50 beam splitter (the reason will be discussed below). For a lossless DC, $P = 1$ for any selected L. In our sample, P slowly decreases as L increases. This result is because the difference between n_1 $(1.318 - 0.004\,26i)$ and n_2 $(1.150 - 0.004\,37i)$ is small; therefore, we are able to achieve a high interference visibility for a small L. For the metal-strip DC used in

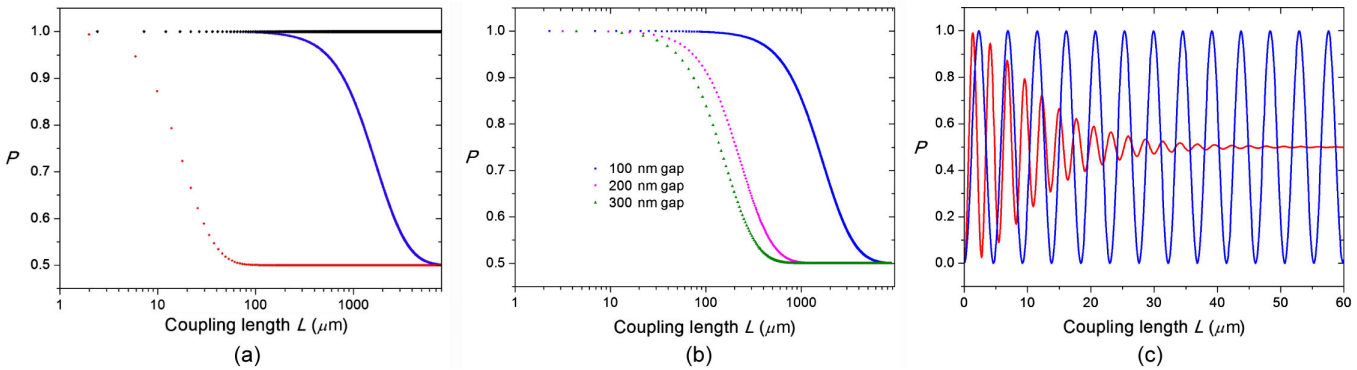

FIG. 5. The relationship between P and the coupling length L. (a) The black, blue, and red dots represent the theoretical calculations for a lossless DC, our DLSPPW DC, and a metal-strip DC [12], respectively. R decreases as L increases and converges to 50% for sufficiently large L in lossy DCs. Here, we use the L values that corresponded to 50:50 beam splitters. (b) Blue, pink, and green dots are numerical calculations of the DLSPPW DC structure with gaps of 100, 200, and 300 nm, respectively. Here, we use the L values that correspond to 50:50 beam splitters. (c) P oscillates with L for our DLSPPW DC (blue line) and the metal-strip DC (red line).

[12], P decreases much faster because the imaginary portion difference between n_1 $(2.036 - 0.02i)$ and n_2 $(1.841 - 0.01i)$ is much larger. Since P is related to $\mathrm{Im}(\Delta n)$ and L, it was possible to tune its decrease speed by adjusting the waveguide gap of our DC structure. When the gap increases, $\mathrm{Im}(\Delta n)$ increases; thus, P decreases more quickly, as shown in Fig. 5(b). The reason why we just consider the L values that correspond to a 50:50 beam splitter is that even for a lossless BS, the HOM interference visibility is related to the splitting ratio. Therefore, for a DC structure, whose splitting ratio depends on the coupling length L and Δn, the interference visibility will oscillate rapidly with L if Δn is constant [see Fig. 5(c)]. With only a 50:50 beam splitter, we can get an ideal visibility of 100%. Thus, to emphasize the influence of loss, we just consider the special L values that correspond to the 50:50 beam splitters.

The absorption loss has been long considered to be the major roadblock for plasmonics to be used for practical applications, so gain medium is often used to compensate for the intensity attenuation of SPPs. However, the first-order coherence of surface plasmon will be destroyed during this absorption and reemission process. Further, our discussion above clearly reveals that loss can also change second-order quantum-interference visibility. The underlying mechanism is that the absorption loss leads to non-Hermitian coupling between plasmons in separated channels, which deviate from the expected Hermitian Hamiltonian description of the system. Therefore, in addition to reducing the absorption loss, special attention should be paid to avoid the non-Hermitian coupling between different channels when designing photonic circuits for a quantum-information process. For example, hybrid structures [5], which use the dielectric waveguide and plasmonic effect together, may be good candidates to reduce this loss effect.

V. CONCLUSION

In summary, we experimentally demonstrate that single plasmons can be used as qubits to perform on-chip quantum-information processing. The discussion presented here regarding loss also introduces a platform for using plasmonic structures to investigate the on-chip quantum-decoherence phenomenon. Additional investigations should consider using single plasmons as qubits to carry quantum information and achieve on-chip linear optical computations or quantum simulations.

ACKNOWLEDGMENTS

This work is funded by NBRP (Grants No. 2011CBA00200 and No. 2011CB921200), the Innovation Funds from the Chinese Academy of Sciences (Grant No. 60921091), NNSF (Grants No. 11374289, No. 10934006, No. 11374288, and No. 11104261), and NCET. We thank Professors Fang-Wen Sun, Bao-Sen Shi, and Zheng-Wei Zhou for useful discussion.

Note added.—Related results have been obtained by two other groups [31,32].

[1] A. Politi, M. J. Cryan, J. G. Rarity, S. Yu, and J. L. O'Brien, Silica-on-silicon waveguide quantum circuits, Science **320**, 646 (2008).

[2] A. Politi, J. C. F. Matthews, and J. L. O'Brien, Shor's quantum factoring algorithm on a photonic chip, Science **325**, 1221 (2009).

[3] W. L. Barnes, A. Dereux, and T. W. Ebbesen, Surface plasmon subwavelength optics, Nature (London) **424**, 824 (2003).

[4] J. A. Schuller, E. S. Barnard, W. S. Cai, Y. C. Jun, J. S. White, and M. L. Brongersma, Plasmonics for extreme light concentration and manipulation, Nat. Mater. **9**, 193 (2010).

[5] C. L. Zou, F. W. Sun, C. H. Dong, X. F. Ren, X. D. Chen, J. M. Cui, Z. F. Han, and G. C. Guo, Broadband integrated polarization beam splitter with surface plasmon, Opt. Lett. **36**, 3630 (2011).

[6] C. H. Dong, C. L. Zou, X. F. Ren, G. C. Guo, and F. W. Sun, In-line high efficient fiber polarizer based on surface plasmon, Appl. Phys. Lett. **100**, 041104 (2012).

[7] E. Altewischer, M. P. van Exter, and J. P. Woerdman, Plasmon-assisted transmission of entangled photons, Nature (London) **418**, 304 (2002).

[8] S. Fasel, F. Robin, E. Moreno, D. Erni, N. Gisin, and H. Zbinden, Energy-time entanglement preservation in plasmon-assisted light transmission, Phys. Rev. Lett. **94**, 110501 (2005).

[9] X. F. Ren, G. P. Guo, Y. F. Huang, C. F. Li, and G. C. Guo, Plasmon-assisted transmission of high-dimensional orbital angular-momentum entangled state, Europhys. Lett. **76**, 753 (2006).

[10] C. K. Hong, Z. Y. Ou, and L. Mandel, Measurement of subpicosecond time intervals between two photons by interference, Phys. Rev. Lett. **59**, 2044 (1987).

[11] G. Fujii, T. Segawa, S. Mori, N. Namekata, D. Fukuda, and S. Inoue, Preservation of photon indistinguishability after transmission through surface-plasmon-polariton waveguide, Opt. Lett. **37**, 1535 (2012).

[12] R. W. Heeres, L. P. Kouwenhoven, and V. Zwiller, Quantum interference in plasmonic circuits, Nat. Nanotechnol. **8**, 719 (2013).

[13] Z. Y. Ou, E. C. Gage, B. E. Magill, and L. Mandel, Fourth-order interference technique for determining the coherence time of a light beam, J. Opt. Soc. Am. B **6**, 100 (1989).

[14] D. J. Bergman and M. I. Stockman, Surface plasmon amplification by stimulated emission of radiation: Quantum generation of coherent surface plasmons in nanosystems, Phys. Rev. Lett. **90**, 027402 (2003).

[15] M. I. Stockman, Spasers explained, Nat. Photonics **2**, 327 (2008).

[16] J. T. Barreiro, T. C. Wei, and P. G. Kwiat, Beating the channel capacity limit for linear photonic superdense coding, Nat. Phys. **4**, 282 (2008).

[17] B. H. Liu, L. Li, Y. F. Huang, C. F. Li, G. C. Guo, E. M. Laine, H. P. Breuer, and J. Piilo, Experimental control of the transition from Markovian to non-Markovian dynamics of open quantum systems, Nat. Phys. **7**, 931 (2011).

[18] S. Longhi, Quantum simulation of decoherence in optical waveguide lattices, Opt. Lett. **38**, 4884 (2013).

[19] S. D. Gupta, and G. S. Agarwal, Two-photon quantum interference in plasmonics: Theory and applications, Opt. Lett. **39**, 390 (2014).

[20] E. Knill, R. Laflamme, and G. J. Milburn, A scheme for efficient quantum computation with linear optics, Nature (London) **409**, 46 (2001).

[21] Y. L. Lim and A. Beige, Generalized Hong-Ou-Mandel experiments with bosons and fermions, New J. Phys. **7**, 155 (2005).

[22] A. Kumar, J. Gosciniak, V. S. Volkov, S. Papaioannou, D. Kalavrouziotis, K. Vyrsokinos, J.-C. Weeber, K. Hassan, L. Markey, A. Dereux, T. Tekin, M. Waldow, D. Apostolopoulos, H. Avramopoulos, N. Pleros, and S. I. Bozhevolnyi, Dielectric-loaded plasmonic waveguide components: Going practical, Laser Photonics Rev. **7**, 938 (2013).

[23] A. Kumar, J. Gosciniak, T. B. Andersen, L. Markey, A. Dereux, and S. I. Bozhevolnyi, Power monitoring in dielectric-loaded surface plasmon-polariton waveguides, Opt. Express **19**, 2972 (2011).

[24] D. Kalavrouziotis, S. Papaioannou, K. Vyrsokinos, A. Kumar, S. I. Bozhevolnyi, K. Hassan, L. Markey, J.-C. Weeber, A. Dereux, G. Giannoulis, D. Apostolopoulos, H. Avramopoulos, and N. Pleros, Active plasmonics in true data traffic applications: Thermo-optic on/off gating using a silicon-plasmonic asymmetric Mach-Zehnder interferometer, IEEE Photonics Technol. Lett. **24**, 1036 (2012).

[25] T. Holmgaard and S. I. Bozhevolnyi, Theoretical analysis of dielectric-loaded surface plasmon-polariton waveguides, Phys. Rev. B **75**, 245405 (2007).

[26] C. L. Zou, F. W. Sun, C. H. Dong, Y. F. Xiao, X. F. Ren, L. Lv, X. D. Chen, J. M. Cui, Z. F. Han, and G. C. Guo, Movable fiber-integrated hybrid plasmonic waveguide on metal film, IEEE Photonics Technol. Lett. **24**, 434 (2012).

[27] C. H. Dong, X. F. Ren, R. Yang, J. Y. Duan, J. G. Guan, G. C. Guo, and G. P. Guo, Coupling of light from an optical fiber taper into silver nanowires, Appl. Phys. Lett. **95**, 221109 (2009).

[28] X. Guo, M. Qiu, J. M. Bao, B. J. Wiley, Q. Yang, X. N. Zhang, Y. G. Ma, H. K. Yu, and L. M. Tong, Direct coupling of plasmonic and photonic nanowires for hybrid nanophotonic components and circuits, Nano Lett. **9**, 4515 (2009).

[29] D. C. Burnham and D. L. Weinberg, Observation of simultaneity in parametric production of optical photon pairs, Phys. Rev. Lett. **25**, 84 (1970).

[30] N. Thomas-Peter, N. K. Langford, A. Datta, L. Zhang, B. J. Smith, J. B. Spring, B. J. Metcalf, H. B. Coldenstrodt-Ronge, M. Hu, J. Nunn, and I. A. Walmsley, Integrated photonic sensing, New J. Phys. **13**, 055024 (2011).

[31] J. S. Fakonas, H. Lee, Y. A. Kelaita, and H. A. Atwater, Two-plasmon quantum interference, Nat. Photonics **8**, 317 (2014).

[32] G. Di Martino, Y. Sonnefraud, M. S. Tame, S. Kéna-Cohen, F. Dieleman, Ş. K. Özdemir, M. S. Kim, and S. A. Maier, Observation of quantum interference in the plasmonic Hong-Ou-Mandel effect, Phys. Rev. Applied **1**, 034004 (2014).